Title

Assessing and minimizing collisions in satellite mega-constellations

Journal

Advances in Space Research, 67(11)

ISSN

0273-1177

Authors

Reiland, Nathan
Rosengren, Aaron J
Malhotra, Renu
et al.

Publication Date

2021-06-01

DOI

10.1016/j.asr.2021.01.010

Peer reviewed

Assessing and Minimizing Collisions in Satellite Mega-Constellations

Nathan Reiland*

Aerospace and Mechanical Engineering, University of Arizona, Tucson, AZ 85721, USA

Raytheon Missiles and Defense, Tucson, AZ 85756, USA

Aaron J. Rosengren

Mechanical and Aerospace Engineering, UC San Diego, La Jolla, CA 92093, USA

Renu Malhotra

Lunar and Planetary Laboratory, University of Arizona, Tucson, AZ 85721, USA

Claudio Bombardelli

Space Dynamics Group, Technical University of Madrid, 2040 Madrid, Spain

Abstract

We aim to provide satellite operators and researchers with an efficient means for evaluating and mitigating collision risk during the design process of mega-constellations. We first introduce a novel algorithm for conjunction prediction that relies on large-scale numerical simulations and uses a sequence of filters to greatly reduce its computational expense. We then use this brute-force algorithm to establish baselines of endogenous (intra-constellation), or self-induced, conjunction events for the FCC-reported designs of the OneWeb LEO and SpaceX Starlink mega-constellations. We demonstrate how these deterministic results can be used to validate more computationally efficient, stochastic techniques for close-encounter prediction by adopting a new probabilistic approach from Solar-System dynamics, as a simple test case. Finally, we demonstrate how our methodology can be applied during the design phase of large constellations by investigating Minimum Space Occupancy (MiSO) orbits, a generalization of classical frozen orbits that holistically account for the perturbed-Keplerian dynamics of the Earth-satellite-Moon-Sun system. The results indicate that the adoption of MiSO orbital configurations of the proposed mega-constellations can significantly reduce risk of endogenous collisions with nearly indistinguishable adjustments to the nominal orbital elements of the constellation satellites.

*Corresponding author

Email addresses: nreiland@email.arizona.edu (Nathan Reiland), ajrosengren@eng.ucsd.edu (Aaron J. Rosengren), renu@lpl.arizona.edu (Renu Malhotra), claudio.bombardelli@upm.es (Claudio Bombardelli)

Keywords: Mega-constellations; Satellite conjunction; Space debris; Frozen orbits; Dynamical evolution and stability

1. Introduction

One of the foremost space science and engineering issues facing society today is conquering Earth's space junk problem, being paramount to managing the increasing orbital traffic in near-Earth space and safeguarding satellite operations (Witze, 2018). This pressing problem is fundamentally connected with the modern fields of space situational awareness (SSA) and space traffic management (STM), which integrate many traditional areas of space research into a single focused topic (National Research Council, 2011, 2012). A major challenge is predicting with sufficient accuracy the location and collision risks of all significant resident space objects (RSOs), a problem that has been compounded in recent years with the launch of numerous small satellites by many nations and the proliferation of orbital debris. The "Kessler syndrome" of collisional cascading, whereby random collisions are predicted to produce new debris at a rate that is greater than the removal rate due to orbital decay, is a more realistic scenario now (Liou and Johnson, 2006) than when it was first proposed in the late 1970s (Kessler and Cour-Palais, 1978). Another emerging concern is the robustness of the current debris mitigation guidelines (Bastida Virgili et al., 2016; IADC, 2017), developed by the Inter-Agency Space Debris Coordination Committee (IADC, 2007, 2019), which were based on the continuation of space traffic at the rates observed in the 1990s. Space traffic, mostly driven by geopolitical and economic factors, has always been subject to considerable fluctuations, but all indications point to a significant increase of traffic in low-Earth orbit (LEO), the most densely populated orbital lanes. OneWeb, SpaceX, and Amazon, in particular, have each submitted ambitious plans to place thousands of satellites in LEO to provide low-latency broadband internet to the world. The full deployment of these "mega-constellations" represents hitherto unknown challenges to the Earth's most congested and contested orbital environment (see, e.g., Fig. 6 in Section 3).

While previous techniques were sufficient to handle past SSA needs, future demands will require new algorithms to build and maintain an expanded space object catalog (SOC), both in quiescent operations and in the presence of a debris-generating event. The only instance of a satellite-satellite collision has been the famed Iridium-Cosmos; given accurate states and detailed maneuver histories of all LEO satellites pre collision, however, the natural question is whether the existing techniques could have actually pinpointed the doom of Iridium. Planned LEO mega-constellations are expected to experience a high volume of collision warnings, as any predicted conjunction less than 1 km could result in a collision avoidance maneuver (Oltrogge and Alfano, 2016). This standard, however, could be problematic in the case of the OneWeb LEO constellation, where, by design, satellites are placed in nearly intersecting, highly inclined orbits, which are known to be prone to self-induced collisions (Swinerd et al., 2004). Moreover, both classic collision-probability techniques, like those of Öpik (1951) and Wetherill (1967), as well as the modern methods used in recent works (e.g., Radtke et al., 2017; Lewis et al., 2017; May et al., 2018; Pardini and Anselmo, 2020) indicate that these closely-spaced objects are at high risk to both endogenous and exogenous threats.

In particular, Radtke et al. (2017) investigated interactions between the space debris environment and the planned OneWeb constellation and found that the highest collision probabilities with background objects will occur during the operational mission, highlighting the need for high rates of post mission disposal. Building on this work, Lewis et al. (2017) investigated the risk of self-induced collisions within the OneWeb constellation using debris evolutionary codes to simulate the impact of the constellation on the orbital environment, and found that over long time spans 25 percent of all collisions could be self-induced. While such studies have highlighted potential issues with mega-constellations, the use of semi-analytical propagators with relatively large output time steps and seemingly unvetted collision-probability models, such as the CUBE method that is based on a significant number of assumptions, could affect the confidence in these results (Lewis et al., 2019). This highlights the need for an accurate means to verify the reliability of such techniques. Furthermore, when large constellations become operational, rigorous conjunction assessments will require the use of accurate orbit and state uncertainty propagation of not only the constellation satellites, but the entire RSO catalogue as well; an otherwise brute-force approach. Such an approach, also accounting for the uncertainty in the state-estimation of each object would represent a formidable task with significant computational requirements,[1] the problem becomes tractable, however, if modern developments in astrodynamics (i.e., regularization, nonsingular orbital element formulations, perturbed collision-probability algorithms, etc.) are properly leveraged with sophisticated computing resources.

It has often been assumed that even the current SOC is too large to permit the application of a highly accurate, brute-force approach to conjunction prediction, and yet, when the planned "space fence" radar network becomes operational, the catalog of tracked objects is expected to exceed one hundred thousand in the coming years (National Research Council, 2011, 2012). Previous brute-force, conjunction-prediction algorithms, although extremely efficient, such as T.S. Kelso's `SOCRATES`[2], have instead relied on simplified analytical orbit propagators that were developed at the time when computing power was far more limited (Hoots et al., 2004; Kelso, 2009). A more recent tool, the "Conjunction Streaming Service Demo" contained in Moriba Jah's `ASTRIAGraph`[3] also currently relies on these simplified propagators, which, together with the two-line elements themselves, cannot yield the required accuracy needed. SGP4 (Simplified General Perturbations 4) (Hoots and Roehrich, 1980; Vallado and Crawford, 2008), for example, uses heavily simplified analytical theories of Brouwer (1959) and Lane and Cranford (1969). Given a satellite state in the mean elements (no short-periodic oscillations) of the TLEs, the secular and long-periodic effects of drag and gravitation are combined with the short-periodic effects of the J_2 zonal harmonic in order to predict the osculating future state of the satellite. This first-order theory is only accurate to order J_2, meaning that even over extremely short time spans the prediction of an object's

[1] A task that is likely being carried out by LeoLabs, although the inner workings of their conjunction-assessment service is not entirely known (Nicolls et al., 2017).

[2] `https://www.celestrak.com/SOCRATES/`

[3] `http://astria.tacc.utexas.edu/AstriaGraph/`

state on the level of meters is by definition impossible with SGP4. In fact, Levit and Marshall (2011) and Vallado (2019) have shown that, even with frequent observations in the form of TLEs, the positional error for a LEO object propagated with SGP4 is, in general, greater than one kilometer. Therefore, if a collision-avoidance maneuver is typically conducted when a conjunction within 1 km is predicted, a system with a consistent uncertainty of 1 km cannot be relied upon to prevent a catastrophic collision, a conclusion dramatically reinforced by the 2009 Iridium-Cosmos event (Kelso, 2009).

In this study, we aim to make a first step towards addressing these concerns by developing a new deterministic, brute-force, conjunction-assessment algorithm, `RICA` (Rapid Integrations for Conjunction Assessment), for use in vetting stochastic collision-prediction techniques as well as in the design of satellite constellations. `RICA` utilizes parallel processing and regularized equations of motion to establish a baseline for the number and severity of endogenous and exogenous conjunctions experienced by the nominal orbital planes within the OneWeb LEO and SpaceX Starlink constellations.[4] The performance of this close-approach-probability algorithm is then evaluated against the baseline predicted by `RICA`. As a final step, and as suggested by Bombardelli et al. (2018, 2020), we consider Minimum Space Occupancy (MiSO) variants of the nominal mega-constellations,[5] which consist of redistributing satellites of different orbital planes in non-overlapping MiSO shells with an altitude separation of 600 meters. The effectiveness of these new design solutions in reducing the number of critical conjunctions is evaluated using `RICA` and `JM`.

2. Problem formulation

2.1. THALASSA, a numerical tool for accurate and rapid orbit propagation

Earth-satellite dynamics is best described by the perturbed two-body problem, which, in Cartesian coordinates, can be stated as $\ddot{\boldsymbol{r}} = -(\mu/r^3)\boldsymbol{r} + \boldsymbol{F}$, where $-(\mu/r^3)\boldsymbol{r}$ is the primary (Keplerian) acceleration and $\boldsymbol{F}$ is the vector sum of perturbing accelerations due to the non-sphericity of the Earth's gravitational field (e.g., J_2), the gravity of external "third" bodies (i.e., lunisolar perturbations), atmospheric drag, solar radiation pressure, etc. Accurate numerical solutions to the perturbed-Kepler problem are often generated through Cowell's method; that is, the integration of the equations of motion in Cartesian coordinates with

[4] It is important to note that the "real" initial placement of these mega-constellation satellites will likely be quite different than those listed in the FCC reports and consequently the goal of this work is not to criticize a "dummy" constellation or even the actual (ever changing and often unknown) orbital designs of the real constellation. Although many sophisticated collision-probability algorithms exist, such as those employed by private companies (e.g., Oltrogge et al., 2018; Alfano and Oltrogee, 2018) and space agencies (e.g., Martin et al., 2004; Bendisch et al., 1997; Liou et al., 2003; Braun et al., 2016), for the purposes of this work, we develop a new, simple technique for estimating the endogenous-collision probability of a set of satellites. This algorithm, the `JM` Approach JeongAhn and Malhotra (2015, 2017), is based on Öpik (1951) and Wetherill (1967) and was chosen over existing methods because of its more straightforward implementation; however, future comparisons should be made against the more standard techniques.

[5] The nominal configurations are those detailed in the most recent FCC filings (no. SAT-LOI-20160428-00041 and SAT-MOD-20181108-00083, respectively).

a numerical solver (the most basic formulation of special perturbation theory). This approach, while simple and robust, is computationally inefficient in comparison to regularized formulations (Baú and Roa, 2020). In particular, the presence of a singularity causes large oscillations in the magnitude of the right-hand side, which are aggravated with increasing eccentricity and unstable error propagation characteristics (Bond and Allman, 1996). These disadvantages can be mitigated or eliminated altogether by employing equations of motion (or formulations of the perturbed two-body problem) that have been regularized (Burdet, 1969; Ferrándiz, 1987; Deprit, 1975).

In regularized formulations, the independent variable is transformed from the physical time to a fictitious time through the generalized Sundman transformation (Berry and Healy, 2002). Using fictitious time as the independent variable gives an immediate advantage: since the fictitious time is an angle-like quantity, meshing the orbit uniformly results in a distribution of points whose density can be adjusted by appropriately choosing numerical parameters. One can select, in particular, a uniform distribution rather than one that is densest at apoapsis, as in Fig. 1. Regularized equations are also stable with respect to the propagation of numerical error, unlike the Cowell method (Roa, 2017), and can be linearized without expressing the perturbations explicitly, thus with no need to truncate expansions in perturbation parameters (Stiefel and Scheifele, 1971). Variation of parameters or projective decomposition can also be employed to obtain regularized, nonsingular sets of orbital elements, which are particularly advantageous for weak perturbations (Peláez et al., 2007; Baú et al., 2015).

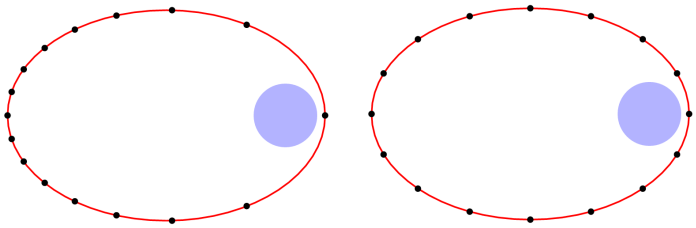

Figure 1: Uniform spacing of points along an orbit in physical (*left*) and fictitious (*right*) time coinciding with the eccentric anomaly. Adapted from Berry and Healy (2002).

A collection of regularized formulations is contained in the `THALASSA` Earth-satellite orbit propagation tool (Amato et al., 2018, 2019, 2020), which is freely available through a GitLab repository.[6] `THALASSA` uses the variable step-size and order (up to 12^{th}) `LSODAR` solver to numerically integrate the equations of motion, which automatically selects the solution algorithm between the implicit Adams-Bashforth-Moulton and backwards differentiation formulas. Even when using such a sophisticated, adaptive solver, regularized formulations have been shown by Amato et al. (2019) to radically improve computational efficiency for long-term propagations.

Figure 2, adopted from Amato et al. (2019), shows that regularized formulations signifi-

[6]URL: `https://gitlab.com/souvlaki/thalassa`.

cantly improve performance with respect to Cowell's in the integration of LEOs, while nearly matching the speed of semi-analytical methods. Moreover, semi-analytical methods, such as the widely-used orbit integration software package, `STELA`, are intrinsically limited in their accuracy due to the approximations introduced in the averaging process (Le Fèvre et al., 2014; Amato et al., 2019). Accordingly, brute-force approaches based on semi-analytical or even less accurate analytical propagators, like `SGP4` and `SDP4` for use with the two-line element sets (Hoots et al., 2004; Levit and Marshall, 2011), cannot consistently achieve the 1 km requisite precision needed to accurately and reliably predict conjunctions (Vallado, 2019).

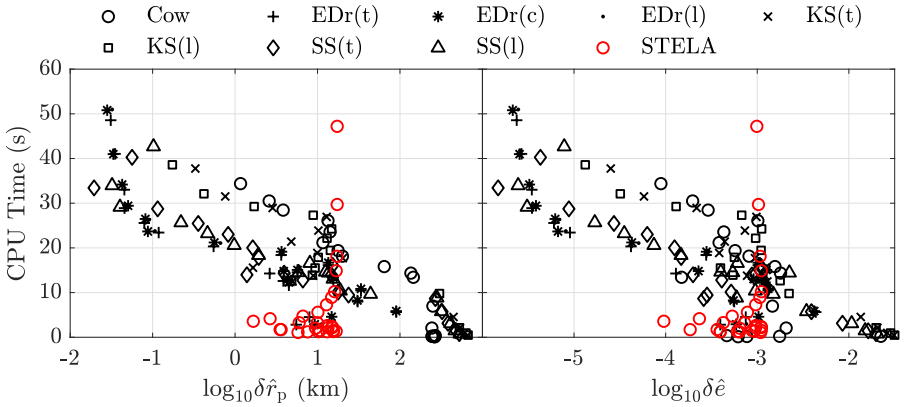

Figure 2: CPU time for 18-year integrations of a LEO against logarithm of error in orbital radius and eccentricity. *Black* and *red circles* denote Cowell integrations and `STELA` propagations, respectively, and other symbols represent various regularized formulations. Adapted from Amato et al. (2019), to which we refer for further details.

The numerical orbit propagation engine in `THALASSA` implements the Kustaanheimo-Stiefel (Stiefel and Scheifele, 1971, ch. 2), Stiefel-Scheifele (Stiefel and Scheifele, 1971, ch. 5), Dromo (Baú et al., 2013; Peláez et al., 2007), and EDromo (Baú et al., 2015) regularized formulations. These formulations are chosen due to their optimal performance in a wide range of dynamical configurations (Roa, 2017; Amato et al., 2019). The equations of motion are integrated with adaptive numerical solvers in modern Fortran.

2.2. The Rapid Integrations for Conjunction Assessment (RICA) algorithm

The developed brute-force algorithm leverages the `THALASSA` orbit propagator (Amato et al., 2019), with the EDromo(l) formulation of the equations of motion (Baú et al., 2015), shown to be the one of the most efficient and precise for the LEO regime (see Fig. 2). We adapt this high-fidelity astrodynamics tool to be highly parallelizable, enabling rapid and accurate propagation of thousands of RSOs.

A given set of "target objects" and potentially impacting "field objects" are passed through three stages of filters that compare the trajectories in order to determine the occurrence of close approaches within some specified distance, τ. First the set containing all

combinations of potentially colliding objects is defined. Next, the vis-viva energy equation,

$$v^2 = \mu \left(\frac{2}{r} - \frac{1}{a} \right), \tag{1}$$

is used to calculate the maximum possible relative velocity, $v_{\max}$, between all objects of the set using the initial osculating orbital elements, where μ is the gravitational parameter of the primary body (Earth), r and v are the satellite's relative position and velocity, respectively, and a is the semi-major axis.

The integration time step is then chosen based on the selected close-approach distance between the target and field objects, τ, according to

$$t_{\text{step}} = \frac{1}{f_s} \left(\frac{\tau}{v_{\max}} \right), \tag{2}$$

where f_s is a factor of safety (typically a value of 1.2 is used). The maximum velocity of the set, $v_{\max}$, is multiplied by a factor of two to represent the relative velocity of two objects in the worst-case scenario. That is, a head on approach where both objects are traveling with the maximum velocity of all objects within the set. Although admittedly conservative, this simple step, whose effect can be seen in Fig. 4, ensures that no close approaches greater than τ will be neglected.

The initial states of the target and field objects are then propagated forward over the time span of interest and the Cartesian separation distance (Euclidean norm), r_{sep}, between each pair of objects at each time step is calculated. Objects with trajectories satisfying $r_{\text{sep}} < \tau$ are passed on to the next stage. Before beginning propagation of the set of objects not eliminated by the previous filter, a new time step of integration is calculated according to Eq. 1 to determine the new v_{max} of the filter stage and a significantly smaller value of τ is chosen. Performing the computations with this structure greatly increases the efficiency of the algorithm without sacrificing accuracy.

This algorithm was implemented using C programming and the MPI message passing interface for parallelization. The resulting program, `RICA` (Rapid Integrations for Collision Assessment), was run on the University of Arizona's High Performance Computing (HPC) cluster on over 200 CPUs. This structure allows for the efficient parallelization of the propagation and trajectory-comparison portions of the code.

2.3. Simple example

To better illustrate the functionality of `RICA`, we investigate a simple test case consisting of an induced artificial collision between five different satellites in a variety of different orbital configurations. As can be seen in Table 1, the initial epoch of the colliding objects is the modified Julian date (MJD) 58834. The collisions are manufactured by backwards propagating with `THALASSA` the target and field objects from the same initial position and epoch (MJD 58849) for a duration of 15 days (Fig. 3). These initial conditions (ICs) are then passed to `RICA` using the same force model and a forward integration time span of 15.1 days (to account for any numerical errors), with close approach values set to $\tau_1 = 1.0$

(km), $\tau_2 = 0.5$ (km), and $\tau_3 = 0.1$ (km), respectively. The effect of selecting a time step according to Equation 2 can be seen clearly in Fig. 4, where relative distances much less than the specified τ between objects are detected. In theory, the approach distance between the target object and each field object should go to zero at a MJD of exactly 58849; however, the presence of numerical error, particularly with backwards propagation, shifts the time of closest approach as well as the minimum approach distance (Fig. 5).

Table 1: Initial Keplerian orbital elements at MJD 58834 of a target and set of field objects for use in demonstrating the `RICA` algorithm. The initial conditions were obtained by backwards propagating these objects from the same position at MJD 58849.

ID	a (km)	e	i (°)	Ω (°)	ω (°)	M (°)
Target	7577.6	0.001	87.9	3.0	45.2	126.8
Field_1	9209.8	0.218	106.3	347.2	56.7	255.5
Field_2	8486.6	0.189	34.7	48.7	224.3	188.5
Field_3	10434.8	0.313	171.4	327.5	256.3	291.2
Field_4	7988.8	0.143	57.1	38.4	59.9	142.7
Field_5	7958.9	0.047	132.2	313.4	316.1	188.3

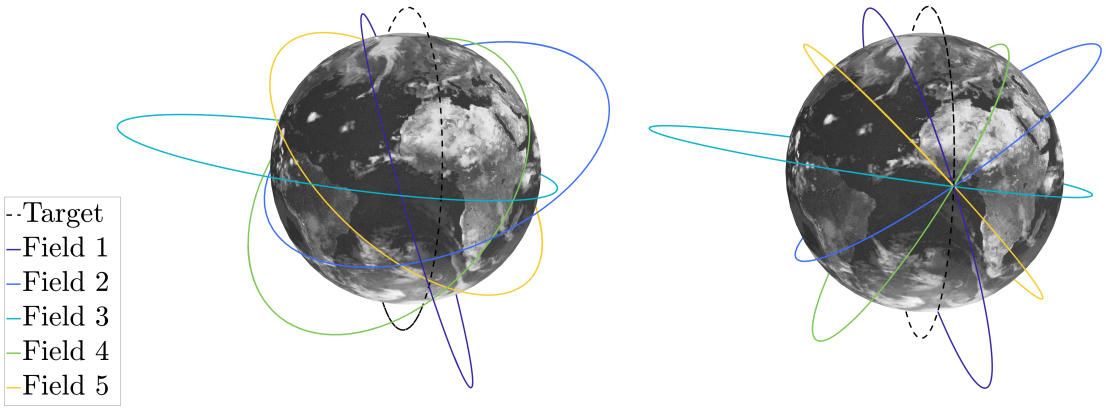

Figure 3: The initial orbits (*left*) at the epoch MJD 58834 and final orbits (*right*) at MJD 58849, the time of manufactured collision, for the `RICA` example objects of Table 1.

2.4. The JeongAhn-Malhotra Approach adapted for circumterrestrial space

The study of orbital collision probability has its roots within Solar System dynamics and was pioneered by Öpik (1951) and Wetherill (1967), respectively, to study collisions within the asteroid belt. The theory begins with the calculation of the collision probability for two intersecting Keplerian orbits, $P_i(\tau, \mathbf{oe}_1, \mathbf{oe}_2)$, which is a function of the orbital elements of the target and field objects, $\mathbf{oe}_1$ and $\mathbf{oe}_2$, respectively, and the collision distance, τ. Here, being Keplerian, the orbits are fixed in space and the mean anomalies are assumed to be independent. Over a long period of time the objects will have a well-defined collision probability at

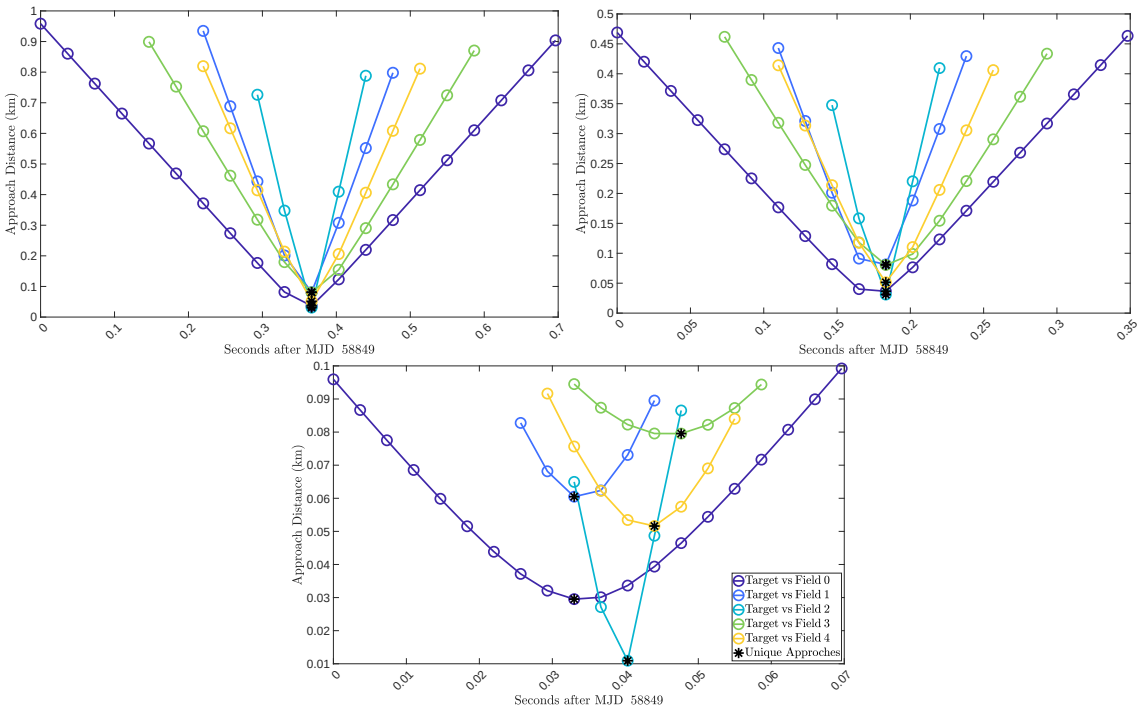

Figure 4: Integration output time steps of 0.0367 seconds (*top left*) and 0.0183 seconds (*top right*) are able to resolve a close approach of 0.0310 km, while an output time step of 0.0037 seconds (*bottom*) can resolve a close approach of 0.0109 km.

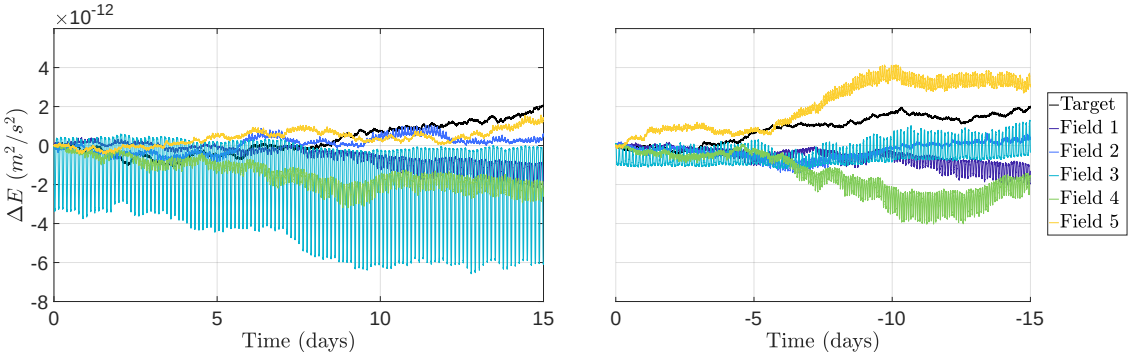

Figure 5: Deviation in the "Hamiltonian" (orbital energy) from its initial value for backwards (*left*) and forwards (*right*) propagation using `THALASSA` with a force model consisting of only the zonal gravity field terms to degree seven.

their intersection. In JeongAhn and Malhotra (2017), a simplified but equivalent derivation of the collision probability of two objects in Keplerian orbits is developed, where the MOID (Minimum Orbital Intersection Distance) is considered to be stochastic and the distribution is assumed to be uniform throughout a sphere of radius τ. The MOID is than averaged in

the range of zero to τ yielding the average probability of collision per unit time:

$$P_i = \frac{\pi \tau U}{2|\boldsymbol{v}_1 \times \boldsymbol{v}_2| T_1 T_2}, \tag{3}$$

where P_i is the collision probability, τ is the collision distance, $\boldsymbol{v}$ is the velocity at the point of closest approach, U is the relative velocity of the objects at the point of closest approach, and T is the orbital period. This theory is then further expanded to account for tangential encounters, which generally have a much higher collision probability. This probability can be computed according to:

$$P_i = 1.7 \cdot T_1 T_2 \frac{\sqrt{(1-k)\tau}}{(1+k) g \sin \alpha}, \tag{4}$$

where $k = |\boldsymbol{v}_2|/|\boldsymbol{v}_1|$ if the objects orbit in the same direction, i.e., both objects are either prograde or retrograde, and $k = -|\boldsymbol{v}_2|/|\boldsymbol{v}_1|$ if they orbit in the opposite sense. Here, α is the angle between the common direction of the two bodies and the positive x-axis, where

$$\sin \alpha = \frac{1 + e \sin f}{\sqrt{(1 + 2e \cos f + e^2)}}, \tag{5}$$

and e and f are the eccentricity and true anomaly, respectively, of either object at the time of closest approach. The determination of whether or not an encounter is tangential is covered in great detail in JeongAhn and Malhotra (2017). It is important to note that in contrast to this approach, many existing techniques for calculating the collision probability between two satellites assume a Gaussian distribution of the intersect distance. While that assumption is likely more appropriate for Earth-orbiting objects (e.g. Patera, 2001; Alfano, 2006; Jones and Doostan, 2013), our goal here is not to introduce a new approach, but rather to demonstrate how one can evaluate its accuracy using brute-force numerical simulations.

To be more applicable to the near-Earth space environment, the probability with respect to an ensemble of fields is required. Past studies using techniques that descended from Öpik (1951) and Wetherill (1967) have in large part been limited to the field of Solar-System dynamics, where the orbital planes of objects typically change at much slower rates and where extremely large sets of objects are considered (the asteroid belt, for example). As such, the semi-major axis (a), eccentricity (e), and inclination (i) of the target and field objects are assumed to be fixed, while the right ascension of the ascending node (Ω), argument of perigee (ω) and τ are assumed to be uniformly distributed stochastic variables. Of course, when considering artificial, Earth-orbiting satellites, such an approach is not suitable as the orbital parameters can change at extremely fast rates and, accordingly, fixing a, e, and i fails to capture the dynamics of the circumterrestrial problem. Following JeongAhn and Malhotra (2015), our solution is to create a distribution of clones by propagating the states of the field and target objects forward with the full dynamics and then randomly sampling the resulting trajectories. In order to keep the problem computationally manageable, only the field objects are cloned, however, the target objects are forward propagated and their trajectories are randomly sampled. Using the Gronchi (2005) algorithm, the MOID for each

pair of target and field objects is calculated. The total collision probability, (P_{total}) of the field and target sets is then computed by summing the individual collision probabilities (3) of all pairs of objects whose MOID is less than or equal to the specified approach distance (Eq. 6),

$$P_{\text{total}} = \frac{1}{N_c} \sum P_i(\boldsymbol{\alpha e}_1, \boldsymbol{\alpha e}_2), \tag{6}$$

where N_c is the multiplicity of field object clones. This complete procedure, implemented using parallel programming and modern Fortan, has been named the "JM Approach", or simply `JM`.

2.5. Frozen orbits and the Minimum Space Occupancy (MiSO)

Frozen orbits correspond to equilibria for the averaged equations of motion, or, as Coffey et al. (1994) candidly remarked, for a system fabricated to represent the averaged orbital behavior of the satellite. Such secular equilibria, under various perturbative environments, have attracted a lot of attention in Earth-satellite missions (e.g. Cook, 1966; Coffey et al., 1994; Chao and Hoots, 2018; Gurfil and Lara, 2013) and planetary satellite and small body orbiters (e.g. Scheeres, 2012; Nie and Gurfil, 2019). In near-Earth space, where the dominant perturbation arises from planetary oblateness, the existence of frozen orbits is attributed to the dynamical balancing of the secular effects of the even zonal harmonics with the long-periodic perturbations of the odd zonal harmonics (Cook, 1966; Chao and Hoots, 2018). These types of orbits with stationary perigee and eccentricity, on average, are of special interest because they minimize altitude variations using only the natural dynamics. Accordingly, as they reduce station-keeping requirements and maintain the relative configuration of clusters of satellites (Gurfil and Lara, 2013), frozen orbits would be ideal in mega-constellation design.

Nominal operational orbits are realized by their osculating elements, not the mean elements used in the determination of frozen-orbit conditions, and consequently the short-period effects must be readmitted to obtain the precise initial conditions. This readmission of the small fluctuations of short period that the averaging process had removed is done using the transformation from mean-to-osculating elements (e.g., Brouwer, 1959). The question arises as to whether the secular equilibria will "unfreeze" when short-term variations are included or when the averaging is pushed to higher order, or when other perturbing effects are taken into account. Although the frozen-orbit definition is tied to the averaged equations of motion, these stationary solutions when recast in osculating space can also be identified as periodic orbits in the meridian plane of the satellite, and as quasi-periodic in the three-dimensional space (Broucke, 1994). The direct computation of frozen, periodic orbits can thus be performed directly from the non-averaged equations, and, when accounting for other perturbations, must be done using an optimization routine.

Strictly speaking, the tesseral harmonics in the geopotential coupled with non-gravitational perturbations destroy the frozen-orbit conditions of the zonal-only problem. This realization has lead to a significant generalization of frozen orbits that we designate the Minimum Space Occupancy (MiSO) orbits (Bombardelli et al., 2018, 2020). In particular, we use the `THALASSA` orbit propagator with a sufficiently complex force model to search for the perturbed-Keplerian orbits that trace out the least amount of volume in three-dimensional

space. We note that if we adopt only the zonal-harmonics model in our algorithm, then the MiSO solutions degenerate to the classical frozen orbits.

3. Numerical experimental setup

3.1. Mega Constellations in the context of the current satellite-debris field

The addition of the OneWeb LEO and SpaceX Starlink mega-constellations alone will increase the number of objects in LEO by 46 percent (Fig. 6), according to the designs described in their most recent FCC filings that actually contain constellation orbit designs (no. SAT-LOI-20160428-00041 and SAT-MOD-20181108-00083, respectively). We note that there have been additional files since, particularly for Starlink, but these do not contain sufficient technical information (i.e. orbital element values) on the new design to permit the type of study performed herein.

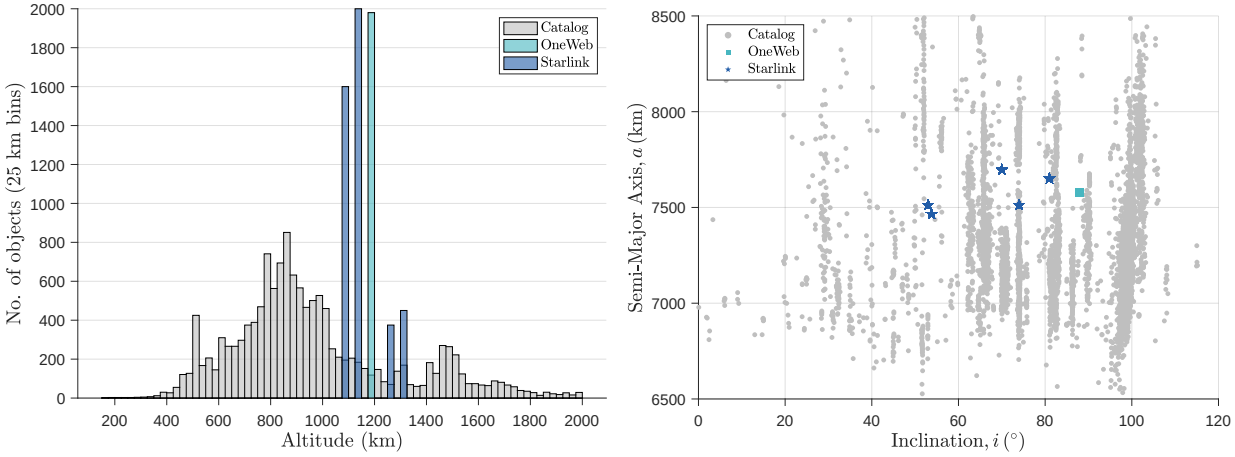

Figure 6: Altitude distribution (*left*) and (i, a) scatter plot (*right*) of the OneWeb LEO and SpaceX Starlink mega-constellations, as obtained from FCC filings no. SAT-LOI-20160428-00041 and SAT-MOD-20181108-00083, respectively, against the background cataloged satellites and debris in low-Earth orbit. ('Norad' Resident Space Object Catalog. www.space-track.org. Assessed 27 Nov. 2019)

3.2. Physical model

We adapt in this study a basic physical model that encompasses the gravity field of the Earth up to the 7th degree and order of the spherical harmonics, the third-body gravity of the Sun and Moon, as well as atmospheric drag using the NRLMSISE-00 model, variable F10.7 solar flux, solar radiation pressure (SRP) with a conical Earth shadow. The physical parameters of the OneWeb and Starlink satellites, needed for the computation of the non-gravitational effects, are given in Table 2. These physical parameters are based on common values of C_D and C_R as well as a brief description of the OneWeb satellite bus found on the Airbus website.[7] For consistency and due to a lack of information, these same parameters

[7] https://www.airbus.com/newsroom/press-releases/en/2019/07/

were imposed upon the satellites of the Starlink constellation. The effects that the model fidelity has on our results is given in 7, which indicate that although the severity and time of closest approach vary slightly with changes in physical model, the general trend of frequency and magnitude of close approaches is preserved.

Table 2: Physical parameters of OneWeb LEO and Starlink constellation satellites used in their respective case studies.

A/m (m^2/kg)	Drag Area (m^2)	SRP Area (m^2)	C_D	C_R
0.0123	1.84	1.84	1.28	1.00

3.3. OneWeb LEO and Starlink case studies and their MiSO variants

The OneWeb LEO and Starlink constellation parameters were obtained from the FCC filings no. SAT-LOI-20160428-00041 and SAT-MOD-20181108-00083, respectively. As can be seen in Tables 3 and 4, OneWeb LEO is composed of 36 orbital planes with 1980 total satellites, while Starlink, the much larger constellation, is composed of 83 planes with 4425 satellites in total. Although these particular configurations are the focus of this study, we remind that it is not our intent to critique any particular design, but rather to showcase the practical implementation of numerical techniques such as `RICA` and `JM`, as well as to demonstrate how MiSO configurations can significantly mitigate the endogenous collision risks associated with mega-constellations.

The generation of the MiSO variants of the OneWeb LEO and Starlink constellations begins with determining a single optimized initial condition of one satellite in each orbital plane. These initial conditions are then propagated forwards in time using a high-accuracy force model for one orbital period. The ICs of the individual satellites in each respective orbital plane are then generated by sampling this orbital period at intervals where the mean longitude ($\varpi = \Omega + \omega + M$) of the MiSO IC matches the mean longitude of the corresponding satellite in the nominal constellation. Using this technique, the MiSO variants of the OneWeb LEO (Fig. 7) and Starlink (Fig. 8) constellations are generated that are nearly indistinguishable from their nominal counterparts. Indeed, the initial conditions of the MiSO satellites are so similar to those of the nominal that the ground tracks of both sets are nearly identical. Of course they are not an exact match as shown in Fig. 8. Here, where the ground tracks of the MiSO variant are placed on top of those of the nominal, it can be seen that the MiSO satellite of Plane 5 is slightly "slower" than the nominal satellite due to a difference in altitude. Although we are not privy to the operational requirements of Starlink, we do not expect this small discrepancy to cause much concern; especially since such a near frozen-orbit design potentially allows the operators to avoid costly station-keeping maneuvers.

Tables 5 and 6 list the initial osculating elements of the nominal constellations and their MiSO counterparts. Only one plane of OneWeb and one plane of each distinct shell of Starlink are shown. Note that in the nominal circular orbit case, the argument of perigee is technically undefined (only the combination of ω and M is meaningful). The greatest differences between the nominal and MiSO configurations is the osculating semi-major axis.

This is the result of the short-periodic fluctuations and how the MiSO ICs are generated from the optimized condition by propagating and sampling over one orbital period.

Table 3: The initial orbital plane configuration of OneWeb LEO, as reported in FCC filings no. SAT-LOI-20160428-00041.

a (km)	e	i (°)	Ω (°)	ω (°)	Planes
7578	0	87.9	0 - 180	0	36

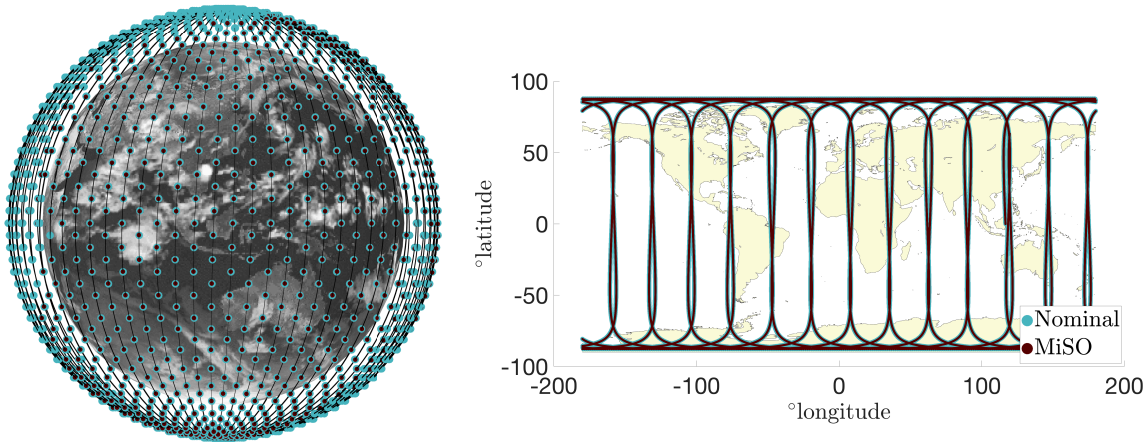

Figure 7: The initial osculating orbital elements at MJD 58849 of the nominal (green) and MiSO (red) variants of one plane of the OneWeb LEO constellation. The mean anomalies of the satellites distributed within these planes range between 0 and 360°.

3.4. Endogenous vs exogenous conjunctions

We consider an "endogenous" conjunction/collision to be one where both parties in the event belong to the same constellation (i.e., self induced), whereas an "exogenous" collision is between a constellation satellite and any other RSO that is not also a member of the constellation, including active and inactive satellites, as well as defunct man-made debris. For this study, due to limitations on the High-Performance Computing (HPC) CPU hours provided by the University, when investigating endogenous conjunctions an all-on-all style analysis was not performed, however any company capable of deploying such a constellation, or government agency required to regulate space traffic, would surely have access to the CPU hours needed to perform such an analysis.

For the OneWeb endogenous case study, we select one plane as the set of target objects (Table 5) and designate the remaining satellites as the field objects. Similarly, because the Starlink constellation is composed of five unique "shells" or plane types of distinct combinations of altitude and inclination, we designate five target planes (Table 6), one from each shell, where the remaining constellation satellites are considered the field objects for each corresponding target plane. The target planes for both the nominal and MiSO Starlink constellations are shown in the *top-right* panel of Fig. 8. The endogenous collision

Table 4: The initial orbital plane configuration of each shell of the SpaceX Starlink constellation, as reported in FCC filings no. SAT-MOD-20181108-00083.

a (km)	e	i (°)	Ω (°)	ω (°)	Planes
7512.4	0	53	0 - 348.8	0	32
7465.9	0	53.8	0 - 354.4	0	32
7696.7	0	70	0 - 300	0	6
7512.4	0	74	0 - 315	0	8
7650.8	0	81	0 - 288	0	5

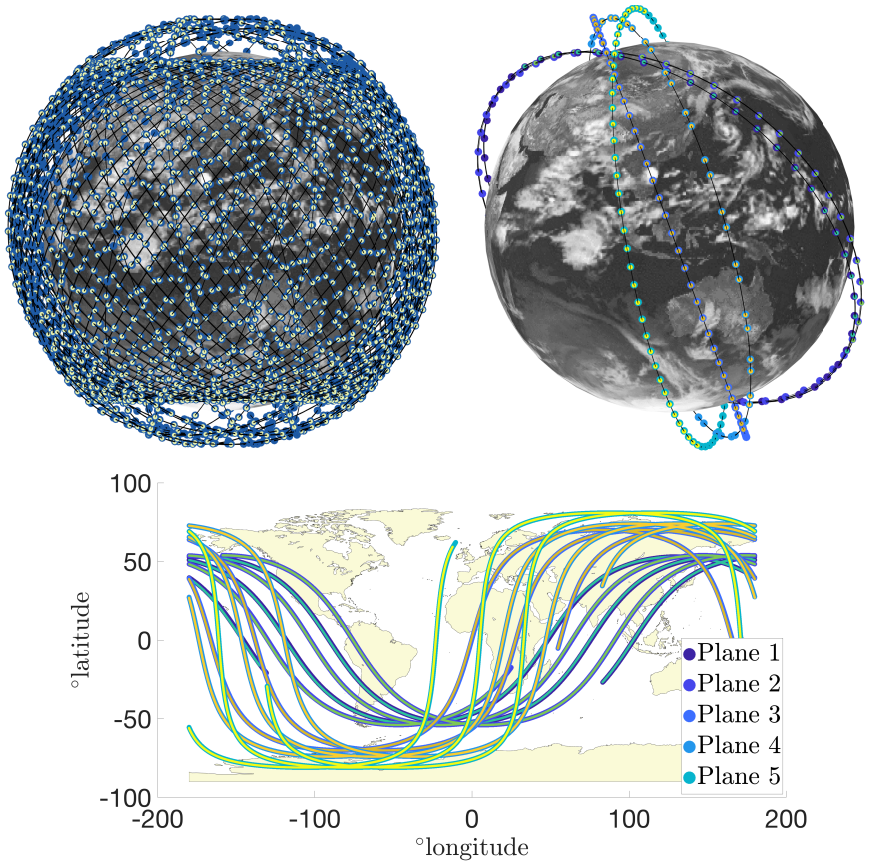

Figure 8: The initial conditions of the nominal (blue) and MiSO (green) variants of the SpaceX Starlink constellation (*top*), as well as their corresponding ground tracks (*bottom*). Note that only the ground tracks of one plane in each shell, as depicted in the *top-right* panel, is shown.

risk of these target planes with respect to the rest of the field objects is then investigated utilizing the aforementioned `RICA` and `JM` numerical algorithms. Importantly, the results of the numerical investigation with `RICA` do not represent the collision risk of the entire constellation, however, they can be used to compare the risk of different configurations as well as evaluate the accuracy of `JM`.

In order to study the risk of exogenous collisions, the entire publicly available SATCAT was obtained from Space-Track.org (see, e.g., Fig. 6). The 18381 different objects were first converted from mean elements to osculating elements in the J2000 frame and then propagated using `THALASSA` to the reference epoch of the study, MJD 58849. These objects were then designated to be the field objects for the exogenous portion of the study with the same considered target planes. The collision risk of these sets of target and field objects are then computed using `RICA` (see §6). The results of this portion of our study must be taken with a grain of salt, as we do not account for the large, and often unknown, state uncertainties of the TLEs.

Table 5: The initial osculating orbital elements at MJD 58849 of the nominal and MiSO variants of one plane of the OneWeb LEO constellation. The mean anomalies of the satellites distributed within these planes range between 0 and 360°.

ID	a (km)	e	i (°)	Ω (°)	ω (°)
Nominal	7578	0	87.9	0	0
MiSO	7557.6 - 7575.0	0.0004 - 0.0026	87.900 - 87.903	359.97 - 359.98	16.0 - 358.0

Table 6: The initial osculating orbital elements at MJD 58849 of the nominal and MiSO variants of one plane of each shell of the SpaceX Starlink constellation. The mean anomalies of the satellites distributed within these planes range between 0 and 360°.

ID	a (km)	e	i (°)	Ω (°)	ω (°)
Nominal 1	7512.4	0	53	348.8	0
MiSO 1	7539.7- 7550.8	0.0003- 0.0014	53.00 - 53.03	348.50 - 348.74	49.9 - 131.6
Nominal 2	7465.9	0	53.8	354.4	0
MiSO 2	7501.8 - 7513.2	0.0003 - 0.0015	53.80 - 53.83	354.13- 354.37	51.2 - 130.1
Nominal 3	7696.7	0	70	300	0
MiSO 3	7704.6 - 7719.8	0.0003 - 0.0018	70.00 - 70.02	299.86 - 299.99	9.0 - 353.3
Nominal 4	7512.4	0	74	315	0
MiSO 4	7507.0 - 7523.3	0.0004 - 0.0022	74.00 - 74.02	314.88 - 314.99	19.3 - 348.6
Nominal 5	7650.8	0	81	288	0
MiSO 5	7654.3 - 7671.2	0.0004 - 0.0024	81.00 - 81.01	287.93 - 287.99	8.5 - 354.1

4. Endogenous assessment of the OneWeb LEO constellation

In the endogenous assessment of the OneWeb LEO constellation, a time span of interest of 90 days is considered with close-approach distances of $\tau_1 = 20$ km, $\tau_2 = 5$ km, and $\tau_3 = 1$ km, respectively, for the first, second, and third filters. This time span was selected because it is computationally tractable, while still permitting the study of the relatively long-term dynamical evolution of the constellations. We also neglect any constellation maintenance

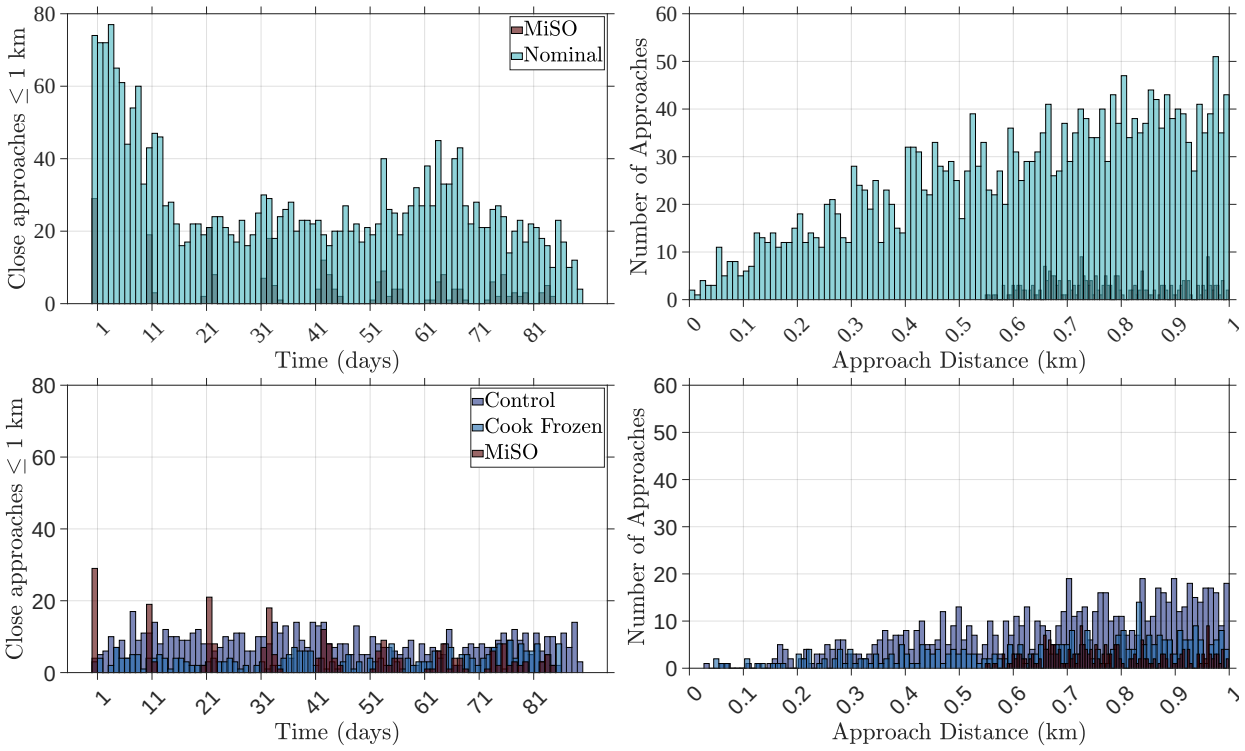

Figure 9: Frequency of close approaches within 1 km (*left*) and close-approach distance (*right*) for the nominal (*top*) and control (*bottom*) configurations of the OneWeb LEO constellation compared against the MiSO counterpart.

during this period, and thus consider only the natural dynamics. Running on the UA's HPC cluster with over 200 CPUs for 13 hours registered a staggering 2,522 unique close approaches of less than 1 km within the nominal case, as well as a minimum approach distance of 6.4 m. As seen in Fig. 9, as many as 75 close approaches of 1 km or less occur on a single day within the nominal configuration. The periodic spikes in the frequency of close approaches experienced by the constellation is equivalent to the period of $\Delta(\omega + M)$ of the approaching target and field objects, which changes as the satellites become increasingly perturbed. This can be seen in Fig. 10 where the time history of the parameter, $\Delta(\omega + M)$, for each pair of objects that eventually experience a close approach is plotted. The lines represent the time history of this parameter, while the dots indicate its value at the time of closest approach.

The MiSO variant of the OneWeb LEO constellation is then evaluated following the same procedure. In stark contrast to the nominal configuration, after 90 days of operation, the MiSO variant only experiences 232 close approaches within 1 km with a minimum approach distance of 550 m (Table 7). Although MiSO significantly outperforms the nominal configuration, it is not without its flaws. The periodic spikes in the close-approach frequencies could be cause for concern, fortunately they are quite predictable since they occur when $\Delta(M + \omega) = 0$ and $\lambda = \pm i$, which is the maximum/minimum latitude λ that the satellites can experience and is the location of the MOID. Furthermore, the approach distances experienced by the MiSO variant are always in excess of 0.5 km, whereas the nominal variant

Table 7: The number of endogenous close approaches within 1 km and the minimum approach distance experienced by the OneWeb LEO constellation after 90 days of operation, compared against the control case and MiSO variant.

ID	Number of Approaches	Minimum Approach Distance (km)
Nominal	2522	0.0064
Control	762	0.0353
Cook Frozen	327	0.0519
MiSO	232	0.5502

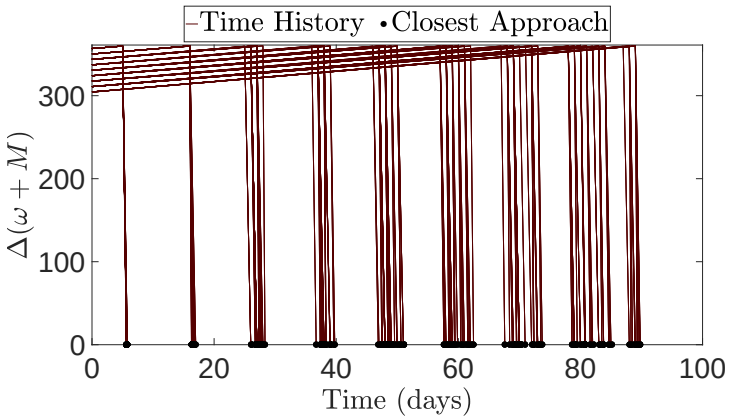

Figure 10: Close approaches within the OneWeb MiSO satellites only occur when the difference in $\omega + M$ of the target and field satellites is zero. As the orbits become more perturbed from their initial configuration, the frequency with which this occurs becomes increasingly less consistent.

experiences approaches as low as 6 m, which would pose a far more significant threat. Recall that the MiSO variant of the OneWeb constellation is generated using one optimized initial condition for each orbital plane, and such that the difference in initial altitude of the adjacent planes is 600 m. In order to test whether or not the reduced frequency and magnitude of close approaches experienced by the MiSO configuration was caused by the frozen nature of the orbits, or merely due to the difference in altitude between the planes, several control cases were also investigated. The orbital elements for the first control case, simply referred to as "Control", are identical to the nominal configuration with the exception that the altitude of the planes is modified to match the altitudes of the initial conditions used to generate the MiSO constellation. Additionally, a second control case is required to rigorously test whether or not a classically frozen constellation is able to reduce the frequency and severity of close approaches to the same extent as the MiSO variant. In this second control case, designated here as "Cook-Frozen", the initial conditions of the constellation are generated by freezing the orbital elements of the previous control case according to Cook (1966) using an FFT-based algorithm to perform the conversion from mean to osculating elements (Ely, 2015).

As indicated by Fig. 9, the MiSO variant significantly outperforms the Control and Cook-

Frozen constellations, showing that simply spacing out the planes and and using the nearest frozen orbit is not sufficient to minimize risk. The special nature of our MiSO design is shown in Fig. 11, where after 90 days of propagation, the variation in periapsis altitude is smallest for a MiSO configuration satellite. Thus, divergence in perigee altitude from an initial condition is an excellent proxy for the amount of volume an orbit will consume. Fig. 11 therefore strongly suggests the superiority of one configuration of the OneWeb constellation with respect to one another. It is clear that the MiSO configuration has both the lowest median and maximum values of variation in the perigee altitude, while the Cook-Frozen variant comes in second place on both counts. Of course, simply plotting this parameter is insufficient to prove that one constellation will experience fewer conjunctions than another. For example, both the control and nominal configurations appear quite similar despite the fact that the nominal configuration experiences far more conjunctions. Additionally, from Fig. 9, we can see that although the Cook-Frozen configuration outperforms both the nominal and control cases, it lacks the most remarkable characteristics of the MiSO variant; namely, the bounding of the all close approaches to about 500 meters and the predictable periodicity of close approaches.

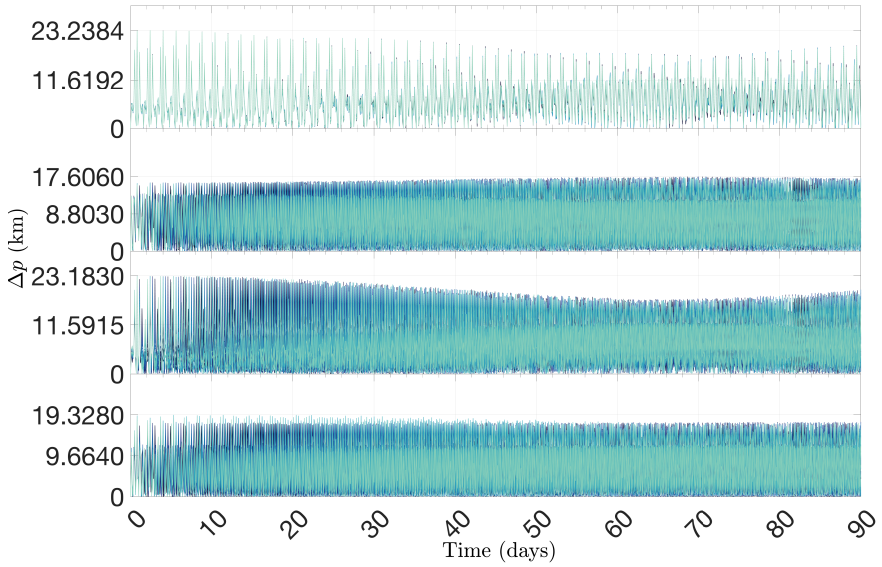

Figure 11: Comparison of the evolution of the divergence from the initial altitude of periapsis of a satellite in each plane of the nominal (*top*), MiSO (*upper middle*), and Control case (*lower middle*), and Cook-Frozen (*bottom*) configurations of the OneWeb LEO constellation.

The performance of `JM` can be seen in Fig. 12. In both the nominal and MiSO cases, the probabilities of both the 100 and 1000 clone runs agree quite well. Furthermore, for the nominal case, `JM` does a reasonably good job at predicting the probability of approaches that occur between 0 and 0.25 km and extremely well at predicting approaches beyond this range; however, it performs quite poorly for the MiSO configuration, for approaches of all distances other than 0.05 km (where it accurately captures the low probability of approach). The inability of `JM` to predict the probability of approaches greater than 0.05 km unfortunately

indicates that the method is not sensitive enough to respond to subtle differences between the nominal and MiSO configurations.

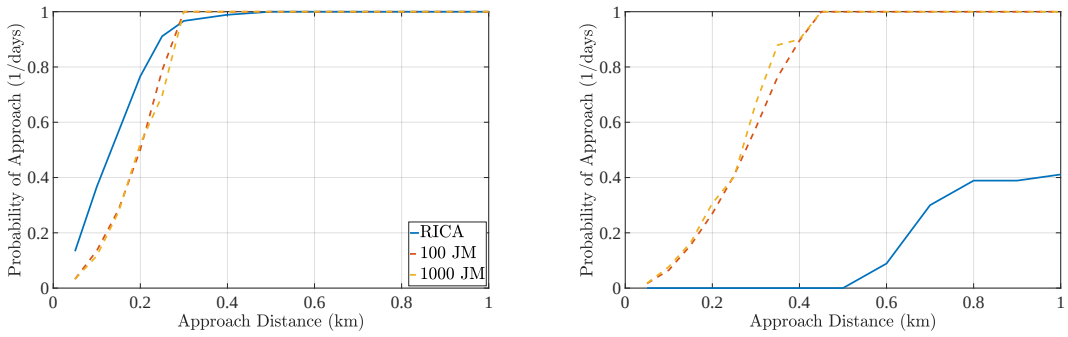

Figure 12: Comparison of the collision probability of the OneWeb nominal (*left*) and MiSO (*right*) configurations.

5. Endogenous assessment of the SpaceX Starlink constellation

To investigate the collision risk of the Starlink constellation, each set of target and field satellites for both the nominal and MiSO variants (Table 6) were run with `RICA` and `JM` for a time span of 90 days. In this case, due to the increase in objects considered, the average time required by a `RICA` analysis of each plane was 40 hours. Fig. 13 shows that every nominal Starlink target plane has a significantly smaller minimum approach distance than their MiSO counterparts, with the statistics provided in Table 8. Additionally, with the exception of Plane 5, every MiSO plane experiences less total close approaches than the nominal versions of the same planes.

Table 8: The number of endogenous close approaches within 1 km calculated by `RICA` and the minimum approach distance experienced by the SpaceX Starlink constellation after 90 days of operation, compared against the MiSO variant.

ID	Number of Approaches	Minimum Approach Distance (km)
Nominal 1	940	0.0167
MiSO 1	135	0.4482
Nominal 2	783	0.0631
MiSO 2	182	0.3938
Nominal 3	539	0.0172
MiSO 3	375	0.2515
Nominal 4	1068	0.0728
MiSO 4	312	0.2612
Nominal 5	346	0.0584
MiSO 5	454	0.3968

In Fig. 13, we see the same periodicity in the frequency of close approaches in the MiSO variants of the Starlink target planes that was observed in OneWeb (Fig. 9). Fig. 14 shows

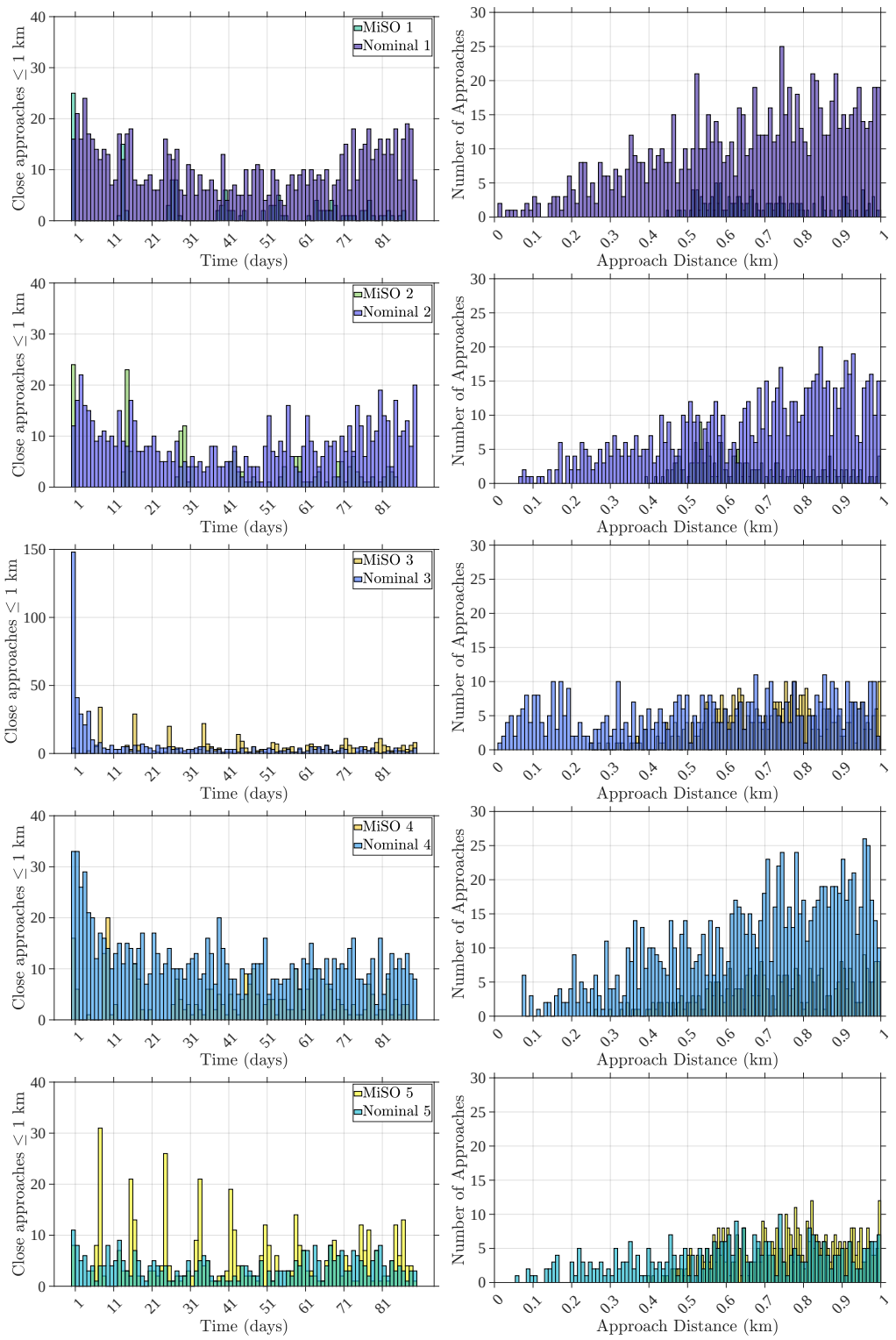

Figure 13: Frequency of close approaches within 1 km (*left*) and close-approach distance (*right*) for each shell of the SpaceX Starlink constellation compared against the MiSO counterpart.

that every close approach experienced by the satellites of the MiSO target Plane 1 occur near the maximum/minimum latitudes of the target satellites (±50°). Although there is certainly an abundance of approaches at these same latitudes in the nominal target plane, there are also a significant number of approaches in the range between −50° and +50°. Investigating further, in Fig. 15, we notice that close approaches only occur when the difference in $\omega + M$ between the approaching target and field objects is around 355°. Initially, when the orbits of the target and field objects have not been significantly perturbed, the target and field objects approach one another at latitudes of ±50° with $\Delta(\omega + M) = 355°$ at a regular interval. In contrast to the OneWeb MiSO constellation (Fig. 10), we see in Fig. 15 that approaches occur at other values $\Delta(\omega + M)$, not just 360°. This same phenomenon occurs in everey target plane of the Starlink MiSO constellation and is a result of approaches occurring between satellites of non-adjacent orbital planes or adjacent planes which have a relatively large difference in Ω. Despite this difference, the periodicity of close approaches also decays in the Starlink MiSO target planes as the orbits are increasingly perturbed. The change in $\dot{M}$ and $\dot{\omega}$ of each satellite is distinct and therefore the moments when the approach conditions ($\Delta(\omega + M)$ and λ) are met no longer occur at the same interval and this previously observed periodicity of close approaches is slowly destroyed.

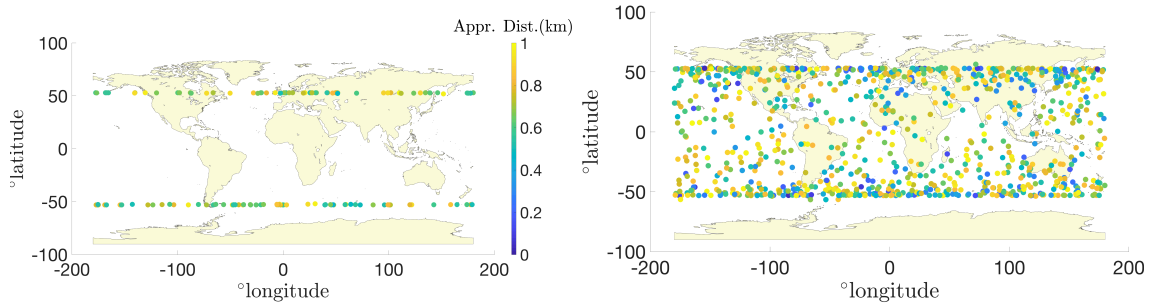

Figure 14: Latitude and longitude coordinates of the target satellites during close approach for the MiSO (*left*) and nominal (*right*) configurations.

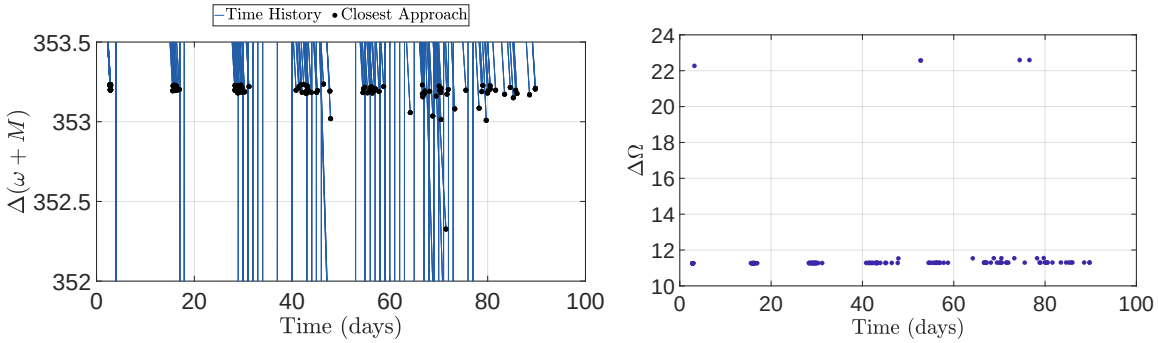

Figure 15: Close approaches within the Starlink MiSO satellites only occurs when the difference in $\omega + M$ of the target and field satellites is near zero. As the orbits become more perturbed from their initial configuration, the frequency with which this occurs becomes increasingly less consistent.

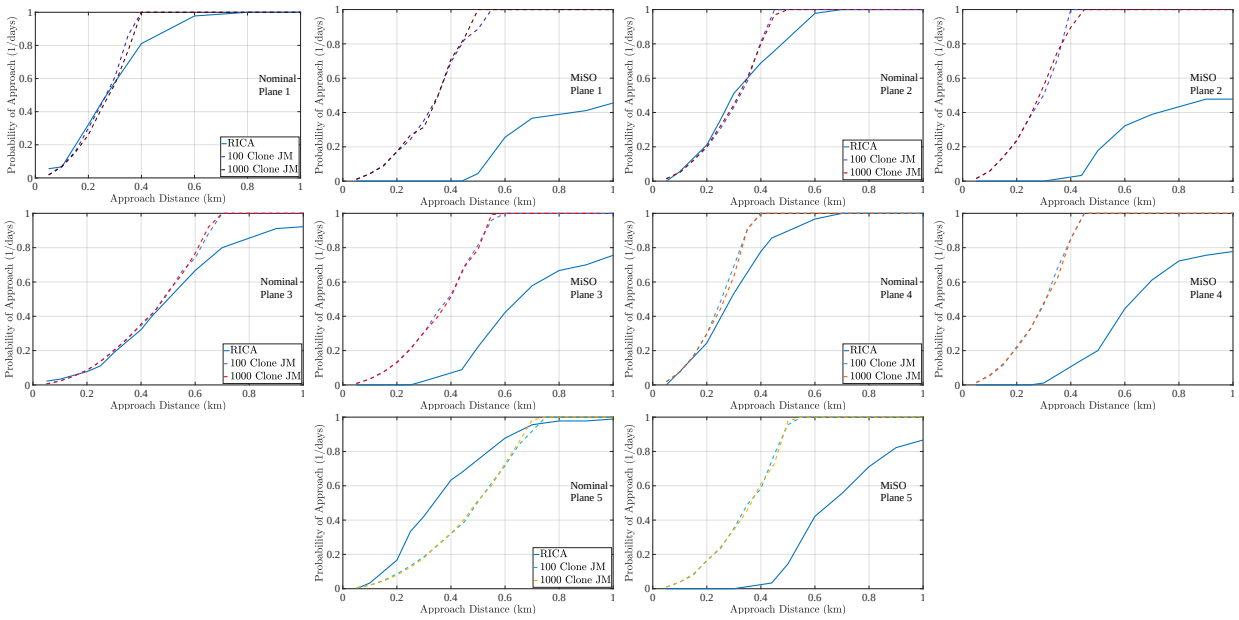

Figure 16: Comparison of the collision probability of the Starlink nominal (*left*) and MiSO (*right*) target planes with their respective fields.

Overall, the performance of `JM` for the nominal Starlink constellation is similar to its performance for OneWeb, in both nominal and MiSO cases. In Fig. 16, we see that for Planes 1 and 2 and for approach distances from 0 to 0.35 km and from 0.6 to 1 km, `JM` performs extremely well, but for the approach distances in between, the probabilities predicted by `RICA` and the `JM` diverge quite significantly. For Plane 3, the performance is excellent between 0 and 0.45 km, but for larger distances `JM` suffers. In Plane 4, we see good performance until about 0.2 km and in Plane 5 the performance is quite poor for the vast majority of approach distances. Finally, as in the OneWeb case study, `JM` is fairly inaccurate for every MiSO target plane.

6. Exogenous assessments

For the exogenous assessment, only the nominal target planes of the OneWeb LEO and Starlink constellations were considered. The reason for this is the similarity between the orbits of the satellites of the nominal and MiSO constellations with respect to the TLE catalog. As in the endogenous assessment, the target plane of the OneWeb constellation and target planes 1 through 5 of the Starlink constellation were run with `RICA` against the entire set of obtained TLEs for a duration of 90 days with $\tau_1 = 20$ km, $\tau_2 = 5$ km, and $\tau_3 = 1$ km. Fig. 17 and Table 9 show that the OneWeb target plane only experiences 63 close approaches with a minimum approach distance of 0.1426 km. Because this is only one plane of the constellation, we could estimate that the remaining 35 planes would likely experience a similar number of close approaches. Likewise in Fig. 18 and Table 9 we see that each Starlink target plane experienced a similar number of close approaches to the OneWeb

target plane with similar minimum approach distances. The single exception is the Starlink target Plane 5, which experienced 118 close approaches, which could be due to its location in the semi-major axis and inclination phase space (see, e.g., Fig. 6).

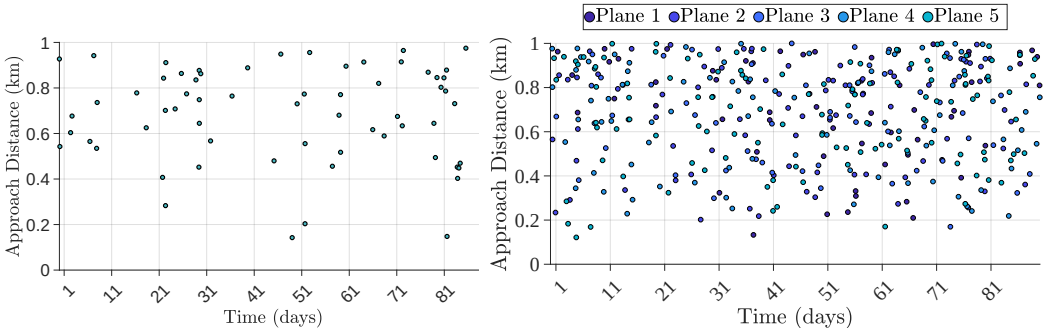

Figure 17: Unique exogenous conjunctions predicted by `RICA` between the nominal OneWeb (*left*) target plane and SpaceX Starlink target planes (*right*) with 18381 public SATCAT RSOs.

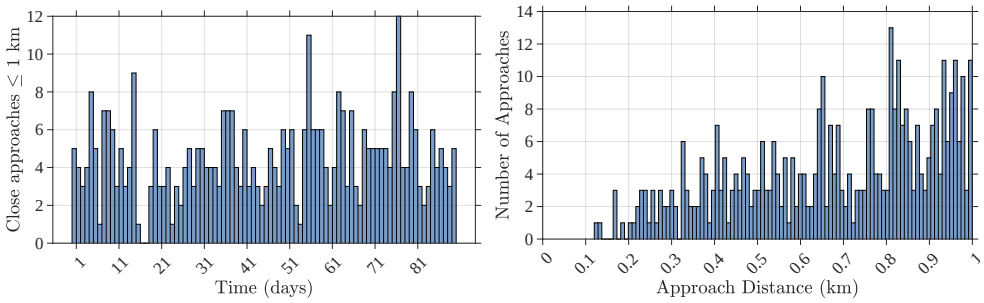

Figure 18: Frequency (*left*) and distance of (*middle*) `RICA`-predicted close approaches experienced between all five nominal Starlink target planes and public SATCAT RSOs

Table 9: Close approaches with exogenous objects experienced by the target planes of the nominal Starlink and OneWeb LEO Constellations.

ID	Number of Approaches	Minimum Approach Distance (km)
OneWeb	63	0.1426
Starlink 1	60	0.1330
Starlink 2	86	0.2020
Starlink 3	59	0.1698
Starlink 4	82	0.2188
Starlink 5	118	0.1215

7. Sensitivity study

In order to determine what effect variations in the force model would have on the close approaches predicted by `RICA`, a sensitivity study was conducted using five different force

models in the THALASSA propagator. The first model was the nominal one used for all RICA and JM assessments previously mentioned in the work, and consists of a 7×7 gravity field, Sun and Moon third-body gravitational perturbations, drag using the NRLMSISE-00 model, variable solar flux, and solar radiation pressure with a conical Earth shadow (Table 3.2). The "low gravity" and "high gravity" models are identical to the nominal model except that they use 3×3 and 20×20 gravity potentials, respectively. The "gravity only" model is the same as the nominal, but does not include any drag or solar radiation pressure forces. Finally a "high area-to-mass ratio" case was investigated where the the same force model as the nominal model was used, however the area-to-mass ratios (A/m) of all the target and field objects were inflated from 0.0123 to 0.0613 kg/m^2. In Fig. 19 it can be seen that the difference in the frequency of approaches and in the experienced approach distances between the nominal (7×7), low gravity (3×3), and high gravity (20×20) are fairly small. Small differences are to be expected, but the the overall structure of the result is preserved. When comparing the gravity only, nominal, and high A/m cases, we can see that the frequency of approaches on each day is extremely similar and the variation in close-approach distances is comparable to what was observed in the comparison between different gravity potentials. Furthermore we notice that the variation between the nominal and High A/m ratio cases was slightly lower than the variation between the gravity only and nominal cases.

8. Discussion

The deployment and management of mega-constellations requires new standards within the fields of SSA and STM, specifically in the realms of satellite observation, conjunction prediction, and sustainable design. Mistakes such as the placement of the Global Navigation Satellite Systems (see, e.g., Rosengren et al., 2015; Daquin et al., 2016) and the failure to predict the Iridium-Cosmos collision will become increasingly costly with the growth of objects in near-Earth space. As we have seen in the endogenous case studies of both the OneWeb and Starlink constellations, techniques that are not purely deterministic may not be sensitive enough to be solely relied upon and should be extensively vetted with a tool such as RICA. For example, the results indicate that although JM is significantly faster than RICA and predicts the endogenous conjunction probability of the nominal OneWeb and Starlink constellations with relatively high accuracy, it is not robust enough to capture the nuanced differences in the dynamics of the nominal versus MiSO constellation variants. The accuracy of the JM technique could be improved by no longer treating time as a stochastic variable, however this would sacrifice the main advantage of the algorithm, its speed, due to the enormous amount of propagations that would be required.

Although accurate close-approach prediction software and collision avoidance maneuvers will be central in preventing endogenous collisions in satellite mega-constellations, the results of the OneWeb and SpaceX case studies indicate that if constellations are intelligently designed, such as our MiSO configurations, collision-avoidance maneuvers could be significantly reduced. This is especially important considering the predicted failure rate of these relatively inexpensively manufactured satellites, where they could potentially become debris hazards within the operational environments of the constellations.

In addition to improving the efficiency of `RICA` and `JM`, an interesting future route is to take the historical high-risk conjunction assessments, reported in the literature and other outlets, and evaluate them under these tools. Future studies could also investigate how recent changes to the designs of these mega-constellation constellations effect endogenous collision rates. Additionally, the effects of stochasticity from mismodeling and uncertainty related to orbital insertion on the initial conditions for the satellites of the MiSO variants of the discussed constellations could be investigated. Such a study could be conducted by varying the initial conditions of the satellites based on some probability distribution and considering the effect of this variation on the results from a simulation with `RICA`. It is important to note that such a study would be extremely computationally expensive unless a much smaller time span of interest were to be considered. Finally, using `RICA` to establish a baseline, an in-depth comparison of the effectiveness of many difference stochastic approaches for estimating collision probability could be conducted and would be very beneficial for the SSA and STM communities.

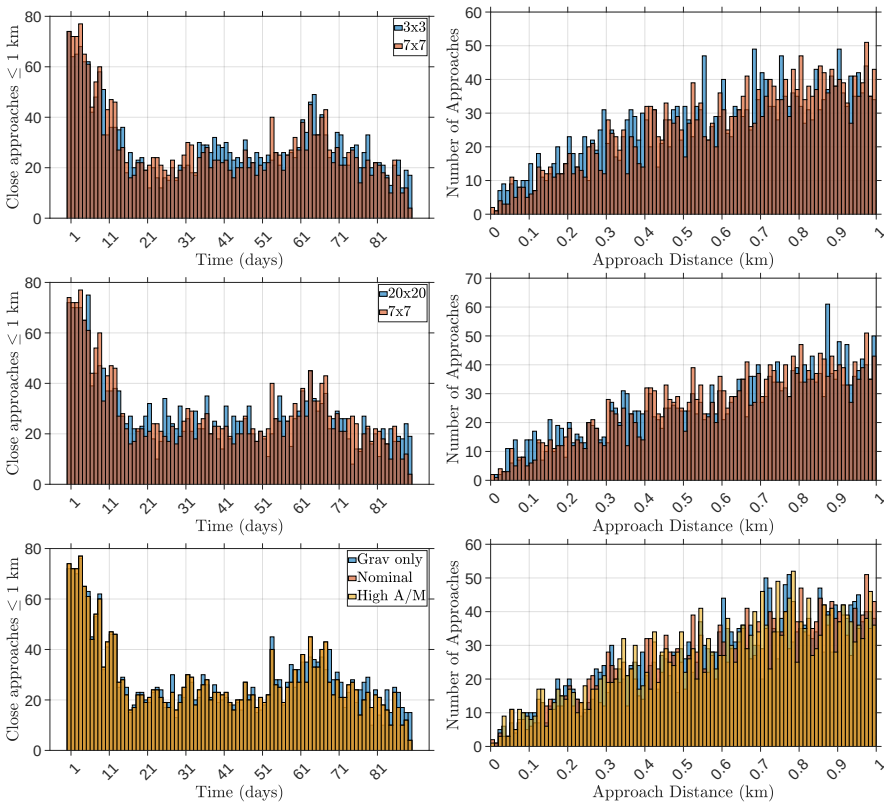

Figure 19: Frequency of close approaches within 1 km (*left*) and close-approach distance (*right*) for the low accuracy (*top*), high accuracy (*middle*) models of the OneWeb LEO constellation compared against the nominal counterpart as well as a comparison of the gravitational-only, nominal, and high area-to-mass ratio models (*bottom*).

9. Conclusion

The RICA brute-force algorithm offers detailed insight into the collision risk of operational satellites, and lends itself as a very useful tool for constellation designers. Although other approaches are faster, it provides a great service vis-a-vis the ability to determine which methods are suited to what scenarios. As an example of this, we determined that the JM approach is not reliable enough to be used as a stand-alone method for evaluating collision risk. This brute-force approach has also been successfully utilized to evaluate subtly different constellation designs. With it, we have demonstrated that the frozen-orbit-based MiSO optimization (Bombardelli et al., 2018) of the nominal OneWeb and Starlink constellations is incredibly effective and could likely reduce the frequency of station-keeping and collision-avoidance maneuvers. We envision that a brute-force approach for conjunction prediction, such as RICA, could be useful in both the design phase as well as in optimizing maneuvers for collision avoidance. However, due to the computational expense of the algorithm, it is not suited for embedded systems, but rather ground-based analysis.

Although we do not know the true designs of the planned mega-constellations, the lack of any currently available astrodynamics tools such as RICA and MiSO (to our knowledge), leads us to assume that the operators of mega-constellations currently have sub-optimal designs in place. It has been demonstrated that simply spacing orbital planes and placing satellites into Cook-Frozen orbits is insufficient with respect to preventing endogenous conjunctions. Additionally, the conducted sensitivity study indicates that this result will hold as long as the physical model includes the effects of tesseral harmonics and dissipative forces. Such dynamical assessments reported herein not only have a profound and tangible influence on satellite constellation design, perhaps attacking the debris problem at its source, but could also provide crucial insight into new satellite and space mission concepts that are not simply predicated by Keplerian motion, but leverage a more complete set of the forces acting within the near-Earth environment.

Acknowledgements

Aspects of this work were presented at the 20th *Advanced Maui Optical and Space Surveillance Technologies Conference*, 2018, Maui, Hawaii and are included in the Master's Thesis of the corresponding author. This research is funded in part by the Universities Space Research Association (USRA) under Grant Agreement SUBK-19-0020 (Subagreement No. 90006.004/08102). N.R. gratefully acknowledges support from the National Science Foundation Bridge to Doctorate Fellowship (NSF 1809591). We especially thank D. Amato, now of the University of Colorado, for his technical contributions to this paper through THALASSA and for inspiring RICA. The numerical routine for the mean-to-osculating transformation was kindly provided by Lamberto Dell'Elce of the Université Côté Azur and Inria Sophia Antipolis Méditerranée.

References

Alfano, S., 2006. Satellite collision probability enhancements. Journal of Guidance, Control, and Dynamics 29, 588–592.

Alfano, S., Oltrogee, D., 2018. Volumetric assessment of satellite encounter rates. Acta Astronautica 152, 891–907.

Amato, D., Bombardelli, C., Baú, G., Morand, V., Rosengren, A.J., 2019. Non-averaged regularized formulations as an alternative to semi-analytical orbit propagation methods. Celestial Mechanics and Dynamical Astronomy 131, 21 (38 pp.).

Amato, D., Malhotra, R., Sidorenko, V., Rosengren, A.J., 2020. Lunar close encounters compete with the circumterrestrial Lidov–Kozai effect: The dynamical demise of Luna 3. Celestial Mechanics and Dynamical Astronomy 132, 35 (18 pp.).

Amato, D., Rosengren, A.J., Bombardelli, C., 2018. THALASSA: a fast orbit propagator for near-Earth and cislunar space, in: Proceedings of the AIAA/AAS Space Flight Mechanics Meeting, AIAA SciTech Forum, Kissimmee, FL, Paper AIAA 2018-1970.

Bastida Virgili, B., Dolado, J.C., Lewis, H.G., Radtke, J., Krag, H., Revelin, B., Cazaux, C., Colombo, C., Crowther, R., Metz, M., 2016. Risk to space sustainability from large constellations of satellites. Acta Astronautica 126, 154–162.

Baú, G., Bombardelli, C., Peláez, J., 2013. A new set of integrals of motion to propagate the perturbed two-body problem. Celestial Mechanics and Dynamical Astronomy 116, 53–78.

Baú, G., Bombardelli, C., Peláez, J., Lorenzini, E., 2015. Non-singular orbital elements for special perturbations in the two-body problem. Monthly Notices of the Royal Astronomical Society 454, 2890–2908.

Baú, G., Roa, J., 2020. Uniform formulation for orbit computation: the intermediate elements. Celestial Mechanics and Dynamical Astronomy 132, 10 (31 pp.).

Bendisch, H.K.J., Sdunnus, H., Wegener, P., Westerkamp, R., 1997. An Introduction to the 1997 ESA Master Model. Second European Conference on Space Debris.

Berry, M., Healy, L., 2002. The generalized Sundman transformation for propagation of high-eccentricity elliptical orbits, in: Proceedings of the AAS/AIAA Space Flight Mechanics Meeting, San Antonio, TX, Paper AAS 02-109.

Bombardelli, C., Falco, G., Amato, D., 2018. Analysis of space occupancy in low-Earth orbit, in: 5th European Workshop on Space Debris Modeling and Remediation.

Bombardelli, C., Falco, G., Amato, D., Rosengren, A.J., 2020. Space occupancy in low Earth orbit. Journal of Guidance, Control, and Dynamics (Submitted).

Bond, V.R., Allman, M.C., 1996. Modern Astrodynamics: Fundamentals and Perturbation Methods. Princeton University Press, Princeton.

Braun, V., Flohrer, T., Krag, H., Merz, K., Lemmens, S., Bastida Virgili, B., Funke, Q., 2016. Operational support to collision avoidance activities by ESA's space debris office. CEAS Space Journal 8, 177–189.

Broucke, R., 1994. Numerical integration of periodic orbits in the main problem of artificial satellite theory. Celestial Mechanics and Dynamical Astronomy 58, 99–123.

Brouwer, D., 1959. Solution of the problem of artificial satellite theory without drag. The Astronomical Journal 64, 378–397.

Burdet, C.A., 1969. Le mouvement Keplerien et les oscillateurs harmoniques. Journal für die reine und angewandte Mathematik 238, 71–84.

Chao, C.C., Hoots, F., 2018. Applied Orbit Perturbation and Maintenance. 2nd ed., Aerospace Press, El Segundo, CA.

Coffey, S.L., Deprit, A., Deprit, E., 1994. Frozen orbits for satellites close to an Earth-like planet. Celestial Mechanics and Dynamical Astronomy 59, 37–72.

Cook, G.E., 1966. Perturbations of near-circular orbits by the Earth's gravitational potential. Planetary and Space Science 14, 433–444.

Daquin, J., Rosengren, A.J., et al., 2016. The dynamical structure of the MEO region: long-term stability, chaos, and transport. Celestial Mechanics and Dynamical Astronomy 124, 335–366.

Deprit, A., 1975. Ideal elements for perturbed Keplerian motions. Journal of Research of the National Bureau of Standards – B. Mathematical Sciences 79, 1–15.

Ely, T.A., 2015. Transforming mean and osculating elements using numerical methods. The Journal of the Astronautical Sciences 62, 21–43.

Ferrándiz, J.M., 1987. A general canonical transformation increasing the number of variables with application in the two-body problem. Celestial Mechanics 41, 343–357.

Gronchi, G., 2005. An algebraic method to compute the critical points of the distance function between two Keplerian orbits. Celestial Mechanics and Dynamical Astronomy 93, 295–329.

Gurfil, P., Lara, M., 2013. Motion near frozen orbits as a means for mitigating satellite relative drift. Celestial Mechanics and Dynamical Astronomy 116, 213–227.

Hoots, F.R., Glover, R.A., Schumacher Jr, P.W., 2004. History of analytical orbit modeling in the U. S. space surveillance system. Journal of Guidance, Control, and Dynamics 27, 174–185.

Hoots, F.R., Roehrich, R.L., 1980. Models for propagation of the NORAD element sets. Project SPACETRACK, Rept. 3, U.S. Air Force Aerospace Defense Command, Colorado Springs, CO.

IADC, 2007. IADC Space Debris Mitigation Guidelines. Technical Report IADC-02-01, Revision 1. Inter-Agency Space Debris Coordination Committee.

IADC, 2017. IADC Statement on Large Constellations of Satellites in Low Earth Orbit. Technical Report IADC-15-03. Inter-Agency Space Debris Coordination Committee.

IADC, 2019. Support to the IADC Space Debris Mitigation Guidelines. Technical Report IADC-04-06, Rev 5.7. Inter-Agency Space Debris Coordination Committee.

JeongAhn, Y., Malhotra, R., 2015. The current impact flux on Mars and its seasonal variation. Icarus 262, 140–153.

JeongAhn, Y., Malhotra, R., 2017. Simplified derivation of the collision probability of two objects in independent Keplerian orbits. The Astronomical Journal 153, 235 (11 pp.).

Jones, B.A., Doostan, A., 2013. Satellite collision probability estimation using polynomial chaos expansions. Advances in Space Research 52, 1860–1875.

Kelso, T.S., 2009. Analysis of the iridium 33-cosmos 2251 collision, in: Proceedings of the Advanced Maui Optical and Space Surveillance Technologies Conference, Maui, HI.

Kessler, D.J., Cour-Palais, B.G., 1978. Collision frequency of artificial satellites: The creation of a debris belt. Journal of Geophysical Research 83, 2637–2646.

Lane, M.H., Cranford, K.H., 1969. An improved analytical drag theory for the artificial satellite problem, in: Proceedings of the AIAA/AAS Astrodynamics Conference, Princeton, NJ, Paper AIAA 69-925.

Le Fèvre, C., Fraysse, H., Morand, H., Lamy, A., Cazaux, C., Mercier, P., Dental, C., Deleflie, F., Handschuh, D.A., 2014. Compliance of disposal orbits with the French Space Operations Act: The good practices and the STELA tool. Acta Astronautica 94, 234–245.

Levit, C., Marshall, W., 2011. Improved orbit prediction using two-line elements. Advances in Space Research 47, 1107–1115.

Lewis, H.G., Diserens, S., Maclay, T., Sheehan, J.P., 2019. Limitations of the cube method for assessing large constellations, in: First International Orbital Debris Conference, Sugar Land, TX, Paper 6104.

Lewis, H.G., Radtke, J., Beck, J., Bastida Virgili, B., Krag, H., 2017. Self-induced collision risk analysis for large constellations, in: Proceedings of the ESA/ESOC Seventh European Conference on Space Debris, Darmstadt, Germany.

Liou, J.C., Johnson, N.L., 2006. Risks in space from orbiting debris. Science 311, 340–341.

Liou, J.C., Kessler, D.J., Matney, M., Stansbery, G., 2003. A new approach to evaluate collision probabilities among asteroids, comets, and Kuiper belt objects, in: 34th Annual Lunar and Planetary Science Conference, League City, TX, Paper 1828.

Martin, C.E., Cheese, J.E., Sánchez-Ortiz, N., Klinkrad, H., Bunte, K., Hauptmann, S., Fritsche, B., Lips, T., 2004. Introducing the esa drama tool, in: Proceedings of the 55th International Astronautical Congress, Vancouver, BC, Paper IAC-04-IAA.5.12.3.

May, S.L., Gehly, S., Carter, B.A., Flegel, S., 2018. Space debris collision probability analysis for proposed global broadband constellations. Acta Astronautica 151, 445–455.

National Research Council, 2011. Limiting future collision risk to spacecraft: An assessment of NASA's meteoroid and orbital debris programs. The National Academies Press, Washington, DC.

National Research Council, 2012. Continuing Kepler's quest: Assessing Air Force Space Command's astrodynamics standards (2012). Committee for the Assessment of the U.S. Air Force's Astrodynamic Standards; Aeronautics and Space Engineering Board; Division on Engineering and Physical Sciences; The National Academies Press, Washington, DC.

Nicolls, M., Vittaldev, V., Ceperley, D., et al., 2017. Conjunction assessment for commercial satellite constellations using commercial radar data sources, in: Proceedings of the Advanced Maui Optical and Space Surveillance Technologies Conference, Maui, HI.

Nie, T., Gurfil, P., 2019. Lunar frozen orbits revisited. Celestial Mechanics and Dynamical Astronomy 130, 61 (31 pp.).

Oltrogge, D.L., Alfano, S., 2016. Collision risk in low Earth orbit, in: Proceedings of the 67th International Astronautical Congress, Guadalajara, Mexico.

Oltrogge, D.L., Alfano, S., Law, C., Cacioni, A., Kelso, T.S., 2018. A comprehensive assessment of collision likelihood in geosynchronous Earth orbit. Acta Astronautica 147, 316–345.

Öpik, E.J., 1951. Collision probabilities with the planets and the distribution of interplanetary matter. Proceedings of the Royal Irish Academy 54, 165–199.

Pardini, C., Anselmo, L., 2020. Environmental sustainability of large satellite constellations in low Earth orbit. Acta Astronautica 170, 27–36.

Patera, R.P., 2001. General method for calculating satellite collision probability. Journal of Guidance, Control, and Dynamics 24, 716–722.

Peláez, J., Hedo, J.M., Rodríguez de Andrés, P., 2007. A special perturbation method in orbital dynamics. Celestial Mechanics and Dynamical Astronomy 97, 131–150.

Radtke, J., Kebschull, C., Stoll, E., 2017. Interactions of the space debris environment with mega constellations – Using the example of the OneWeb constellation. Acta Astronautica 131, 55–68.

Roa, J., 2017. Regularization in Orbital Mechanics: Theory and Practice. De Gruyter, Berlin.

Rosengren, A.J., Alessi, E.M., Rossi, A., Valsecchi, G.B., 2015. Chaos in navigation satellite orbits caused by the perturbed motion of the Moon. Monthly Notices of the Royal Astronomical Society 464, 3522–3526.

Scheeres, D.J., 2012. Orbital Motion in Strongly Perturbed Environments: Applications to Asteroid, Comet and Planetary Satellite Orbiters. Springer-Praxis, Berlin.

Stiefel, E.L., Scheifele, G., 1971. Linear and Regular Celestial Mechanics. Springer-Verlag, Berlin.

Swinerd, G., Lewis, H., Williams, N., Martin, C., 2004. Self-induced collision hazard in high and moderate inclination satellite constellations. Acta Astronautica 54, 191–201.

Vallado, D.A., 2019. Long-term numerical propagation for Earth orbiting satellites, in: Proceedings of the AAS/AIAA Astrodynamics Specialist Conference, Portland, ME, Paper AAS 19-601.

Vallado, D.A., Crawford, P., 2008. SGP4 orbit determination, in: Proceedings of the AIAA/AAS Astrodynamics Specialist Conference, Honolulu, HI, Paper AIAA 2008-6770.

Wetherill, G., 1967. Collisions in the asteroid belt. Journal of Geophysical Research 72, 2429–2444.

Witze, A., 2018. The quest to conquer Earth's space junk problem. Nature 24, 25–26.